

Holistic Simulation for FIREX Project with FI³

T. Johzaki¹, H. Sakagami², H. Nagatomo¹, K. Mima¹

¹ *Institute of Laser Engineering, Osaka University, Suita, Osaka 565-0871, Japan*

² *Theory and Computer Simulation Center, National Institute for Fusion Science, Toki
509-5292, Japan*

e-mail: tjohzaki@ile.osaka-u.ac.jp

In fast ignition research, the clarification of core heating mechanism is one of the most critical issues. To understand and identify the crucial physics in the fast heating, we developed the fast ignition interconnected integrated code FI³ and carried out the core heating simulations for fast heating experiments with cone-guided targets. It was found that the scale length of the pre-plasma at the inner-surface of the cone and the density gap at the contact surface between the cone tip and the imploded core plasma strongly affect efficiency of core heating. When the heating laser is 10^{20} W/cm² and 1ps, the pre-plasma scale length of 1.5 μ m is optimum for the core heating. In this case, the dense core is heated up to 0.86keV. In the double scale length case (long scale of $\sim 5\mu$ m in underdense region and short scale of $\sim 1\mu$ m in overdense region), which is observed at the radiation –hydro simulations for low intensity laser-plasma interactions, the dense core is heated more efficiently than single short scale length cases. The contribution of fast ions to the core heating is also discussed.

INTRODUCTION

In the recent fast ignition (FI) [1] experiments with cone-guided targets [2], the imploded core plasma was heated up to ~ 800 eV with a high coupling efficiency. As the next step, FIREX (Fast Ignition Realization Experiment) project [3] has been started at Institute of Laser engineering, Osaka university. The mechanism of the high coupling in a petawatt laser heating is, however, is not clarified yet. In most of the previous studies for the heating process, laser-plasma interaction (LPI), relativistic electron transport and core heating processes have been individually studied, *e.g.*, relativistic LPI and the fast electron propagation by particle code [4-10] and hybrid code [11-14], and core heating process hybrid code [15,16] and relativistic Fokker-Planck (RFP) code [17,18]. In Ref.[19], though the core heating simulations including LPI were carried out using a collisional PIC code, the imploded core profile was arbitrary. To simulate the overall physics and identify the crucial physics in the fast heating, we developed a multidimensional integrated code system “Fast Ignition Integrated Interconnecting code” (FI³ code) [20, 21], which includes all important physics from the implosion to the core heating. In the FI³ code, the overall implosion dynamics is simulated by an ALE-CIP radiation-hydro code “PINOCO” [22]. A collective PIC code “FISCOF” [20] simulates the relativistic LPI to evaluate the time-dependent energy distribution of relativistic electron beam. The core heating is simulated with a RFP code coupled with hydro-based burn simulation code “FIBMET” [19, 23].

In the previous works [24, 25], on the basis of integrated simulations with FI³ code for fast heating experiments with cone-guided CD shell targets [2], we found the density gap effect on fast electron transport. If the plasma density between cone tip and dense core is low such as $10n_c$ (n_c is a laser critical density), the strong two stream instability is induced there due to fast electron flow, which generates the strong static field. Due to this field at the rear surface of the cone tip, some of fast electrons having relatively low energy are reflected and trapped inside the cone tip and bulk electrons are accelerated toward the cone tip. These confined moderate-energy fast electrons are gradually released from the cone tip with intensity of $\sim 10^{18}$ W/cm² even after finishing laser irradiation and contribute to the core heating. Thus, if such low density plasma exists between cone tip and core plasma, the profiles of fast electrons change during propagation into the core, *i.e.* the energy spectrum is moderated and the electron

beam duration becomes longer. As the results, core heating efficiency becomes high compared with the no density gap case. Even if including the density gap effect, however, the resultant ion temperature reaches only 0.45keV, which is still lower than the value obtained in the experiments (0.8keV) [25].

In the heating phase of FI, before main pulse irradiation, low density plasma is formed on the cone inner surface due to the pre-pulse. In the previous simulations [25], we assumed a scale length of $L_f = 5\mu\text{m}$ for the pre-plasma. However, the scale length strongly depends on the pre-pulse profiles of the heating laser (intensity, duration and focal spot), and it affects the fast electron energy distribution and the coupling from heating laser to fast electron. In the present paper, in addition to the density gap effect, hence, we evaluate the pre-plasma scale length dependence of core heating efficiency using FI³ code.

At the relativistic LPI, in addition to fast electrons, fast ions are generated. We also evaluate the possibility of the accelerated ions for contributing to the core heating.

SIMULATION CONDITION

The details of FI³ code consisting of three codes (an ALE Radiation-hydro code ‘‘PINOCO’’, a collective PIC code ‘‘FISCOF’’ and a coupled Relativistic-Fokker-Planck and hydro code ‘‘FIBMET’’ are described in the previous papers [18, 20- 24]. The procedure of the present core heating simulations for a cone-guided target is as follows. First, we carried out implosion simulations for an Au cone attached CH shell target using PINOCO to obtain the compressed core profile. For heating phase, time-dependent profiles of fast electron and ion generated by the heating laser irradiation are evaluated with PIC simulations (FISCOF). The following energy transports into the imploded dense core are simulated by FIBMET where the time-dependent profiles of fast particles evaluated by FISCOF simulations are used as the external sources in RFP code, and the imploded core profiles obtained by PINOCO simulations are used as the initial condition of bulk plasma. In the core heating, the multi-dimensional natures, *e.g.* geometrical effects of laser-cone interactions, magnetic field effects, spatial beam divergence, are off cause important. However, full scale (time and space) multi-dimensional simulations are very expensive. Thus, for the present parametric study on scale length dependence, we used 1-dimensional (1D) PIC and FP codes.

PRE-PLASMA SCALE LENGTH DEPENDENCE

Fast Electron Profiles

For evaluation of fast electron profiles, we carried out 1D PIC simulations for laser-cone tip interactions. In the PIC simulations, electrons and ions (Au, $Z=50$) are mobile and the collision process is not included. The density profile assumed in PIC simulations is shown in Fig.1. The cone tip is modelled by $100n_c$ (n_c is the laser critical density) and $10\mu\text{m}$ thickness plasma. The pre-plasma having exponential density profile ($n_e \propto \exp(x/L_f)$, L_f is scale length and is changed from $0\mu\text{m}$ to $5\mu\text{m}$) is attached to the front surface (laser irradiation side). For introducing the density

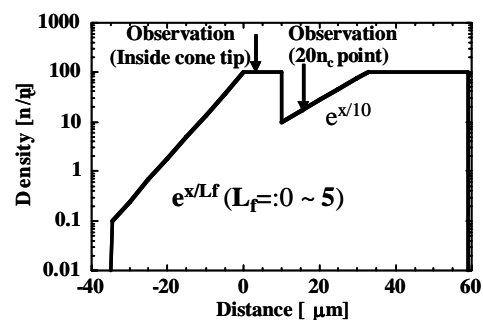


Fig.1 Electron density profile of the cone tip and the imploded plasma assumed in PIC simulation.

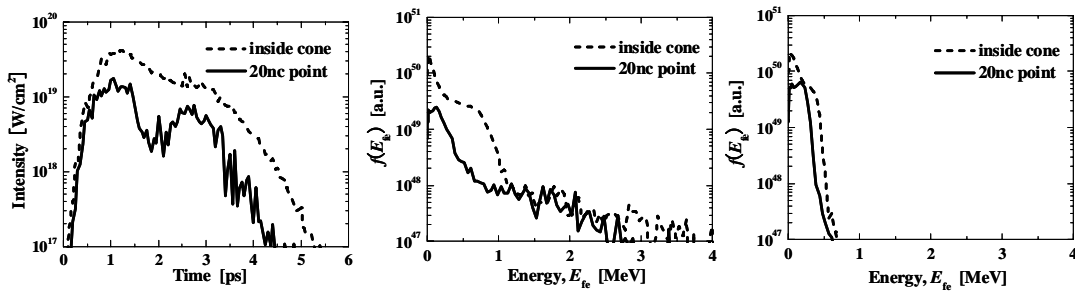


Fig.2 Forward-directed fast electron ($E_{fe} > 100\text{keV}$) profiles observed at the two different points (inside the cone tip and at $20n_c$ point in the imploded plasma) in the case of $L_f = 1\mu\text{m}$. (a) time history of electron beam intensity, (b) energy spectra observed during laser irradiation ($t = 1.0\text{ps} \sim 1.5\text{ps}$) and (c) the spectra after finishing laser irradiation ($t = 2.5\text{ps} \sim 3.0\text{ps}$)

gap on the rear surface of the tip, we located low density imploded plasma, of which density is set to $n_e = 10n_c$ at the contact surface and is exponentially raised up to $100n_c$ at $24\mu\text{m}$ away from the rear surface. Following the imploded plasma, dense core plasma is located with the density of $100n_c$. In the PIC simulation, we assumed Au with $Z=50$ as the bulk ion in the whole region since. The heating laser is the Gaussian pulse with the wavelength of $\lambda_L = 1.06\mu\text{m}$, the pulse duration (full width of half maximum) of $\tau_{FWHM} = 750\text{fs}$ and the peak intensity of $I_L = 10^{20}\text{W/cm}^2$. The irradiated laser energy is $0.79\text{J}/\mu\text{m}^2$, which corresponds to 560J when the laser spot size is $15\mu\text{m}$. The simulation time is 6ps . The forward-directed fast electron profiles are observed at two different points; one is inside the cone tip and the other is at the $20n_c$ point in the imploded plasma.

3.1.1. Density Gap Effect at Rear Surface of Cone Tip

In **Fig.2**, we show the fast electrons ($E_{fe} > 100\text{keV}$) profiles observed in the case of $L_f = 1.0\mu\text{m}$. Fig.2 (a) is the temporal profile of beam intensity, and Fig.2 (b) and (c) are the energy spectra during laser irradiation ($t = 1\text{ps} \sim 1.5\text{ps}$) and after finishing laser irradiation ($t = 2.5\text{ps} \sim 3.0\text{ps}$), respectively. The density gap effect [24, 25] is observed in Fig.2. The higher beam intensity of forward directed electrons in the cone tip than that at $20n_c$ point indicates the confinement of relatively low energy fast electrons inside the cone tip during the laser irradiation. These confinement component is clearly found at the region of $E_{fe} < 1\text{MeV}$ in Fig.2(b). The longer fast electron beam duration than the heating laser duration means the release of the confined electrons from the cone tip after finishing laser irradiation and the energy of these electrons is lower than 1MeV as is shown in Fig.2(c).

In the previous work [25], we assumed the homogeneous density profiles ($100n_c$, $10n_c$ and $2n_c$) for the plasma located at the rear of cone tip. Contrary to this, in the present study, we assumed the exponential profile which seems to be more realistic one. In this case, the bulk ions tend to flow into the lowest density point from the both sides (from the cone tip and the denser imploded plasma region) because of the pressure imbalance. In addition, the static field generated at the rear surface of the cone tip due to the fast electron current pulls ions from the cone tip into the low density plasma. The density gap is hence filled due to these ion flows, which reduces the density gap effect. As the results, the confined electrons are rapidly released from the cone tip. It can be found this phenomenon in the profile of fast electron intensity observed at $20n_c$ point (Fig.2 (a)). There exist two peaks; the first one corresponds to the peak of laser intensity and the second one corresponds to the release of confined electrons resulting

from filling up the density gap. After the second peak, thus, the fast electron beam intensity is rapidly decreased.

3.1.2. Density Steepening at the Laser Irradiation Surface

When the heating laser intensity is high such as 10^{20}W/cm^2 , the pre-plasma is pushed into the dense region by the Ponderomotive force, and then the density steepening takes place. In Fig.3, the Spatial profiles of electron density n_e (blue lines) and phase plots of electrons (light blue dots) observed at $t = 1\text{ps}$ for the three different scale length cases ($L_f = 0.25, 1.0$ and $5.0\mu\text{m}$). In the short scale length cases ($L_f = 0.25\mu\text{m}$ and $1.0\mu\text{m}$), the pre-plasma is almost swept away and the heating laser is directly interacts with the dense cone tip. Under this situation, the returned fast electrons are pushed back into the cone tip by the laser oscillating Ponderomotive force at the LPI region. It is hence observed the periodically-launched forward-directed electron bunches in electron phase plots (Fig.3 (a) and (b)).

3.1.3. Scale Length Dependence

The difference in fast electron profiles due to the pre-plasma scale length is clearly observed in **Fig.3** (a) ~ (c). In a short scale length case ($L_f = 0.25\mu\text{m}$, Fig.3 (a)), the underdense LPI region is narrow, so that the energy coupling efficiency from laser to fast electrons is small, which weakens the density gap effect. In addition, the density steepening rapidly occurs and then the heating laser interacts with dense cone tip from the early stage of laser irradiation. Therefore, though the electron bunches are observed in Fig.3 (a), the accelerated electron energy and forward-directed electron beam intensity are low. With increasing the scale length, the underdense LPI region and a time required for density steepening become long. Thus, before density steepening occurs, more electrons are accelerated and then the confinement due to the density gap effect becomes remarkable. As the results, in the case of $L_f = 1\mu\text{m}$ (Fig.3 (b)), the energies of both forward-directed bunched electrons and returned electrons become high. In the further long scale length case such as $L_f = 5\mu\text{m}$, a time required for density steepening is much longer. As is shown in Fig.3(c), in the case of $L_f = 5\mu\text{m}$, the pre-plasma has not been completely swapped away at $t = 1.0\text{ps}$; the long scale pre-plasma is still remained at the LPI region. Thus, at this moment, the energy of fast electron accelerated at the LPI region is very high compared with the lower scale length cases ($L_f = 0.25\mu\text{m}$ and $1\mu\text{m}$). The most of absorbed laser energy is carried by such high energy electrons and then the current becomes weak, so that the density gap effect also becomes weak. In addition, at the LPI region, the reflection of returned fast electrons becomes weak; the backward acceleration is observed in the underdense region.

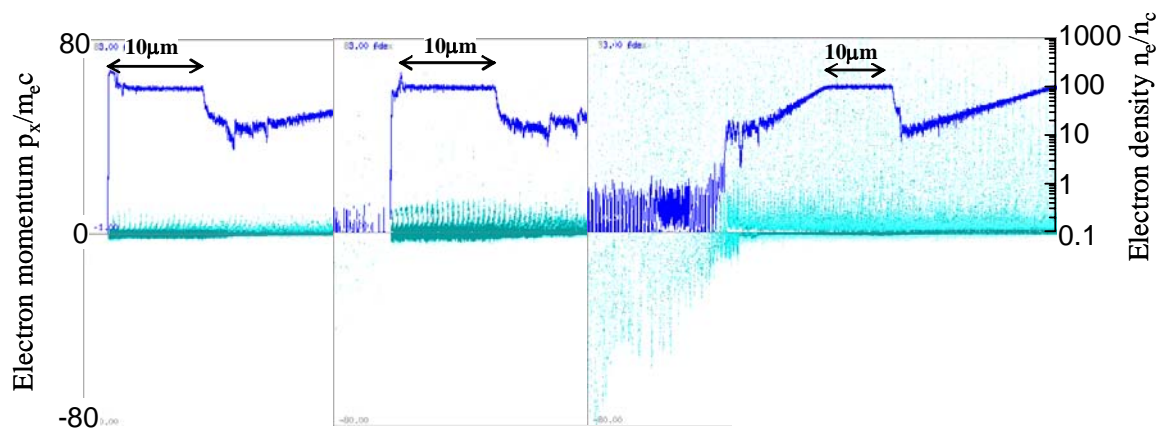


Fig.3 Spatial profiles of electron density n_e (blue lines in log scale at right axis) and phase plots (light blue dots in linear scale at left axis) observed at $t = 1\text{ps}$ for the three different cases ($L_f = 0.25\mu\text{m}, 1.0\mu\text{m}$ and $5.0\mu\text{m}$).

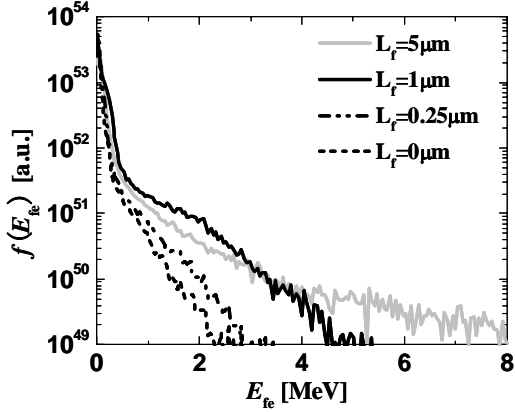


Fig.4 Time-integrated forward-directed fast electron spectra observed at $20n_c$ point in the imploded plasma for the case of $L_f = 0\mu\text{m}$, $0.25\mu\text{m}$, $1\mu\text{m}$ and $5\mu\text{m}$.

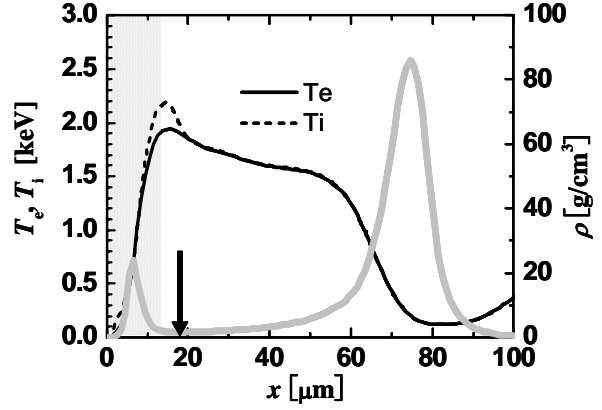


Fig.5 Imploded core at the central axis ($r = 0$) obtained by an r - z cylindrical 2D implosion simulation for Au cone guided CD target. The hatched region is Au and the other is CD. The fast electron injected point is indicated by arrow.

Figure 4 shows the time-integrated forward-directed fast electron spectra observed at $20n_c$ point in the imploded plasma for the cases of $L_f = 0\mu\text{m}$, $0.25\mu\text{m}$, $1\mu\text{m}$ and $5\mu\text{m}$. With increasing L_f from $0\mu\text{m}$ to $1\mu\text{m}$, the underdense LPI region becomes longer, which leads to increasing the energy coupling from laser to fast electrons and the generated fast electron energy. In the case of $L_f = 5\mu\text{m}$, the energy of fast electron becomes higher than those in the short scale length cases. Compared with $L_f = 1\mu\text{m}$ case, the number of electrons is large in high energy region ($E_{fe} > 4\text{MeV}$). However, such a high energy electron has a long range compared with a compressed core size and then does not heat a compressed core efficiently. Contrary to this, the number of relatively low energy electrons, which are mainly contribute to the core heating, is small since the density gap effect and the density steepening effect become weak as was stated above. These results indicate the existence of the optimal scale length for efficient core heating.

Core Heating

Using the time-dependent profiles of fast electron after passing through the low-density gap region, we carried out the core heating simulations using the 1D RFP-Hydro code. As for the initial condition of bulk plasma, we use the imploded core profiles at the central axis ($r = 0$) obtained by r - z cylindrical 2D implosion simulation with PINOCO (**Fig.5**). The fast electrons are injected behind the cone tip.

In **Fig.6**, spatial profiles of fast-electron energy deposition rates at $t = 2.5\text{ps}$ are plotted for the $L_f = 1\mu\text{m}$ case. In the low-density region around the fast electron injection point, the Joule heating is comparable to the collisional heating due to the Coulomb interactions with bulk electrons. In the dense core region, the fast electron current can be easily cancelled by bulk electron flow with small drift velocity ($v_d \ll c$) because of much larger density of bulk electron than that of fast electron, so that the field effect is negligible and the collisional heating is dominant. As for the Coulomb interactions in dense plasmas, not only short-range binary collisions in the impact parameter range of $b_{\min} < b < \lambda_D$ but also long-range interactions ($b_{\min} > \lambda_D$) including the collective shielding effect contribute to the energy deposition of fast electrons. Here, b_{\min} is the minimum cutoff impact parameter, being of the order of the distance of the closest approach, and λ_D is the Debye length. The temporal evolution of ion and electron temperatures averaged over $\rho > 10\text{g/cm}^3$ region, $\langle T_k \rangle = \int_{\rho > 10\text{g/cm}^3} T_k(x) R_{DD}(x) dx / \int_{\rho > 10\text{g/cm}^3} R_{DD}(x) dx$ where k denotes ion or

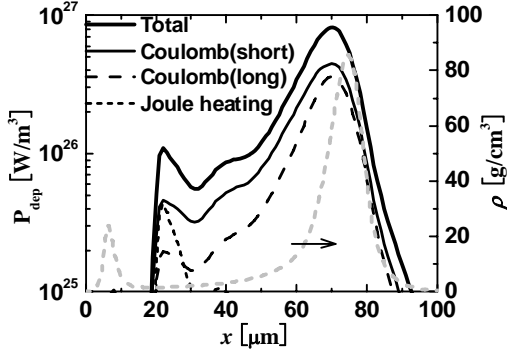


Fig.6 Energy deposition profile of fast electron at $t = 2.5$ ps for the case of $L_f = 1\mu\text{m}$.

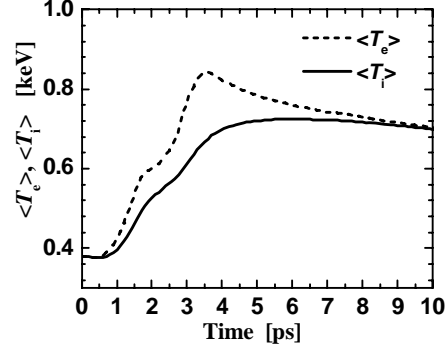


Fig.7 Temporal evolution of ion and electron temperature averaged over dense core region ($\rho > 10\text{g/cm}^3$) in the case of $L_f = 1\mu\text{m}$.

electrons and $R_{\text{DD}}(x)$ is DD reaction rate at position x , are shown in **Fig.7** for the case of $L_f = 1\mu\text{m}$. Due to the collisional heating, the bulk electron is heated first, and then the bulk ion is heated via the temperature relaxation. Thus, the electron temperature reaches maximum ($\langle T_e \rangle_{\text{max}} = 0.84\text{keV}$) at first (at $t = 3.6\text{ps}$), and then $\langle T_i \rangle_{\text{max}} = 0.72\text{keV}$ is obtained by 3ps delay.

The results of core heating simulations by varying L_f are summarized in **Fig.8**. Fig.8 (a) shows the scale length dependence of energy carried by the fast electrons (total and $E_{\text{fe}} < 2\text{MeV}$ component) evaluated by PIC simulations and the energy deposited by fast electron inside the fuel plasma evaluated by the following RFP-hydro simulations. The right axis indicates the energy coupling from laser to each value. In Fig.4 (b), the maximum value of $\langle T_i \rangle$ is plotted as a function of L_f . With increasing L_f up to $1.5\mu\text{m}$, the energy coupling from heating laser to fast electron becomes large, so that the deposited energy and the resultant core temperature increase. The scale length becomes long furthermore, the total beam energy gradually decreases. However, the higher energy component ($E_{\text{fe}} > 2\text{MeV}$) increases, so that the low energy component ($E_{\text{fe}} < 2\text{MeV}$), which is effective in core heating, decreases faster than the total beam energy. As the result, the deposited energy in the fuel plasma and the resultant core temperature also decrease. These results indicate that the core heating efficiency depends not on the total beam energy but on the beam energy of low energy component ($E_{\text{fe}} < 2\text{MeV}$). In the present simulations, the optimum scale length for core heating is $L_f = 1.5\mu\text{m}$. In this case, the energy coupling from the heating laser to the core is 14.9% and ion in the core is heated up to 0.86keV (0.48keV rising).

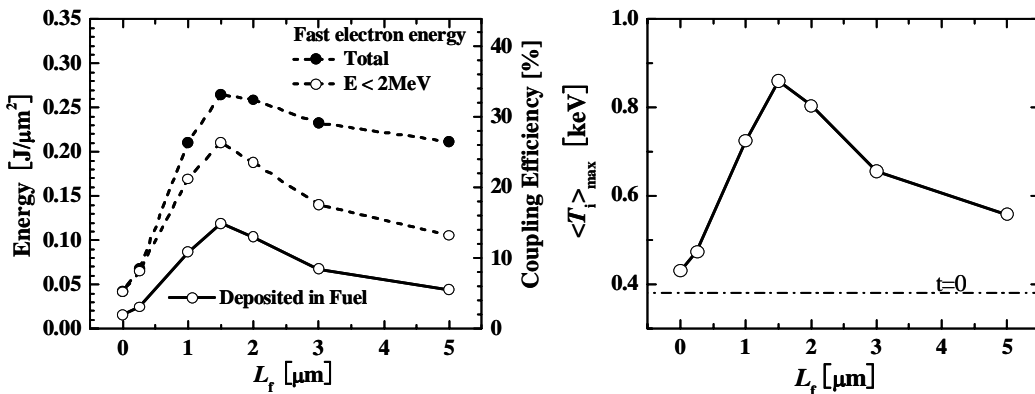


Fig.8 Pre-plasma scale dependence of (a) total fast electron energy, its $E_{\text{fe}} < 2\text{MeV}$ component and deposited energy of fast electron inside the fuel, and (b) maximum value of core ion temperature $\langle T_i \rangle_{\text{max}}$.

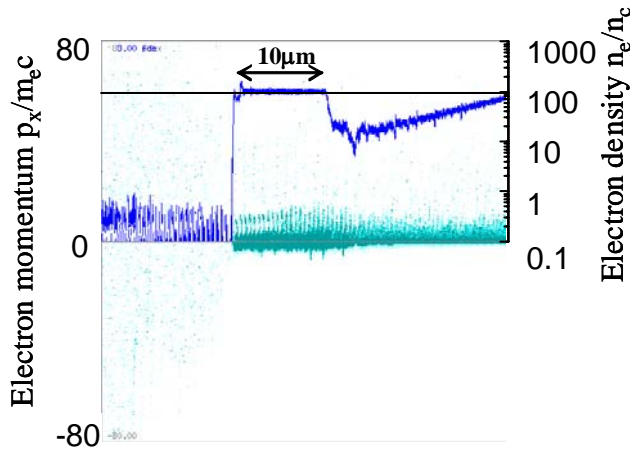


Fig.9 Spatial profiles of electron density n_e (blue lines in log scale) and phase plots (light blue dots in linear scale) observed at $t = 1$ ps for the double scale length case ($L_{fu} = 5\mu\text{m}$ and $L_{fo} = 1\mu\text{m}$).

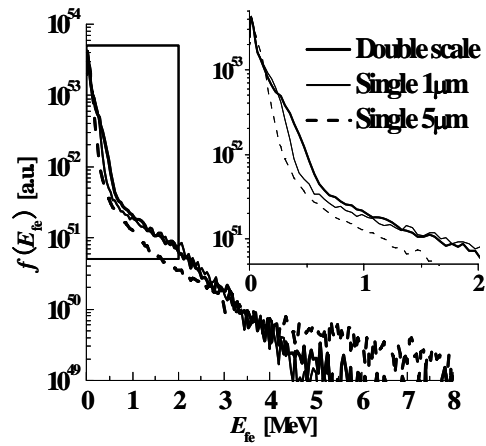


Fig. 10 Time-integrated fast electron spectra for the double scale length case ($L_{fu} = 5\mu\text{m}$ and $L_{fo} = 1\mu\text{m}$) and for the single scale length cases ($L_f = 1\mu\text{m}$ and $5\mu\text{m}$ cases).

Double Scale Length Case

In the above discussion, we assumed single scale-length pre-plasmas, *i.e.*, the density profile of pre-plasma was assumed as $n_e \propto \exp(x/L_f)$ from the underdense region to the $100n_c$ region. The results of radiation-hydro simulations for low intensity laser ($\sim 10^{11}\text{W/cm}^2$) and plasma interactions, however, indicate that the pre-plasma has a double scale-length density profile, *i.e.*, the underdense region has a relatively long scale length ($\sim 10\mu\text{m}$ or more) and the overdense region has a short scale length ($\sim 1\mu\text{m}$). For estimating the core heating properties in such cases, we carried out the simulations by assuming double scale length pre-plasmas. In order to compare with the single scale length cases, the scale length was assumed as $L_{fu} = 5\mu\text{m}$ for the underdense region and $L_{fo} = 1\mu\text{m}$ (or $1.5\mu\text{m}$) for the overdense region.

Figure.9 shows spatial profiles of electron density n_e and phase plot observed at $t = 1$ ps for the double scale length case ($L_{fu} = 5\mu\text{m}$ and $L_{fo} = 1\mu\text{m}$). Compared with the $L_f = 1\mu\text{m}$ single scale length case, the double scale length plasma has the long underdense plasma, so that in the early stage of laser irradiation, more fast electrons are generated. The static field generated at the density gap, thus, becomes slightly stronger, which makes the density gap effect remarkable a little. But, the underdense plasma is rapidly swapped away by the laser Ponderomotive force. As for the density steepening, hence, the scale length of overdense region determines the characteristics, so that the density profile at $t = 1$ ps is almost the same as that in the $L_f = 1\mu\text{m}$ single scale length case.

The time-integrated fast electron spectrum for the double scale length case ($L_{fo} = 1\mu\text{m}$) is plotted in **Fig.10** together with those for the single scale length cases ($L_f = 1\mu\text{m}$ and $5\mu\text{m}$ cases). The spectrum in the double scale length case is similar to that in the single scale length case of $L_f = 1\mu\text{m}$. the spectrum for the double scale length case is almost the same as that in $L_f = 1\mu\text{m}$ single scale case except for the low energy region ($E_{fe} < 2\text{MeV}$). The number of electrons in the low energy region is slightly large in the double scale case because of the increase in the gap effect. Using the fast electron profiles obtained in the double scale cases, the core heating simulations were carried out. The obtained results are plotted in **Fig.11** together with the results of single scale cases. It is found that in the double scale cases, the core heating efficiencies and

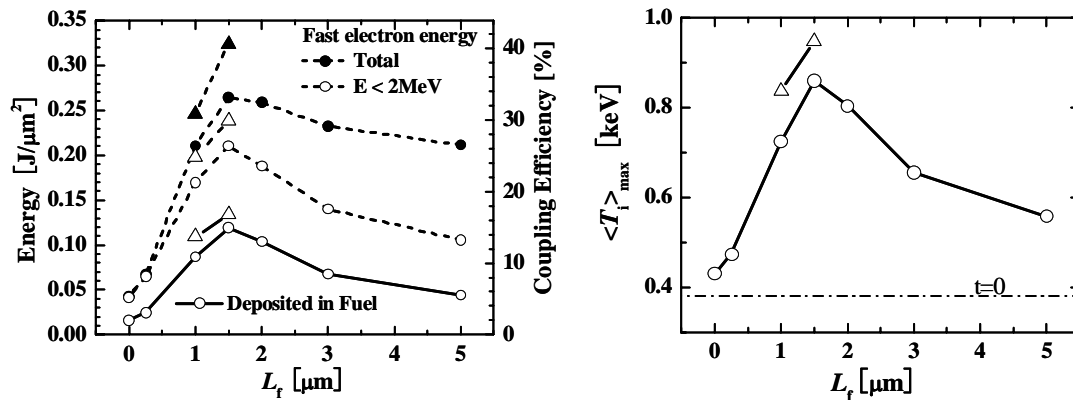


Fig.11 Pre-plasma scale dependence of (a) total fast electron energy (black) and its $E < 2\text{MeV}$ component (blue) and deposited energy of fast electron inside the fuel, and (b) maximum value of core ion temperature $\langle T_i \rangle_{\text{max}}$. The circles are the single scale length cases and the triangles are the double scale length cases.

the resultant core temperatures become high compared with those in the single scale cases because of increase in the electron number in the low energy region ($E_{fe} < 2\text{MeV}$).

Even if the single scale length is assumed, we obtained the heated core temperature comparable to the value obtained at the experiments when $1\mu\text{m} \leq L_f \leq 2\mu\text{m}$. In the case of the double scale length, which seems to be more practical, the core heating becomes more efficiently.

CONTRIBUTION OF FAST IONS

In the intense LPI, the bulk ions are also accelerated. At the LPI region, fast ions are generated by sweeping potential [26]. At the rear side of cone tip, the electric field built up due to the fast electron current acts on the ions to accelerate toward the dense core. Those accelerated ions have the possibility for contributing to the core heating.

In the present PIC simulations, all the ion is assumed as Au with $Z=50$ and irradiated laser intensity is $10^{20}\text{W}/\text{cm}^2$. The maximum ion energy obtained by PIC simulations is $\sim 600\text{MeV}$, which well agrees with the scaling for the acceleration by sweeping potential [26]. On the other hand, the ions accelerated at the rear surface are accelerated up to $\sim 100\text{MeV}$. The energy coupling efficiency from laser to fast ions is $0.6\% \sim 2.3\%$ for the single scale length case ($L_f = 0\mu\text{m} \sim 5\mu\text{m}$). However, the range of such a high- Z and heavy ion is too short to heat the dense core. The range of 500-MeV (100-MeV) Au ion ($Z=50$) evaluated with continuous slowing down model is $0.027\text{g}/\text{cm}^2$ ($0.0083\text{g}/\text{cm}^2$) in a CD plasma ($T = 1\text{keV}$, $\rho = 50\text{g}/\text{cm}^3$). The accelerated ions hence deposit their kinetic energies and momenta in the cone tip and the low density imploded plasma before reaching the dense core. As the results of core heating simulations including the fast ion transport, where the fast ion beams evaluated by PIC simulations are injected at the same point as the electron beam injection point, all the fast ion stopped in the low density imploded plasma and does not contribute to the core heating.

CONCLUDING REMARKS

On the basis of the FI³ integrated simulations, we evaluated the core heating properties of cone-guided targets. From the simulations where the density profile of pre-plasma was described by the single scale length from underdense region up to solid density and the density

gap was located at the rear surface of cone tip, we found that the core heating efficiency is very sensitive to the pre-plasma scale length and there exists the optimum scale length.

At the LPI region, the density steepening occurs due to the strong laser Ponderomotive force. In the too short scale length case ($\ll 1\mu\text{m}$), the underdense plasma is rapidly swapped away and the steepening occurs quickly. Thus, the energy coupling from laser to fast electron and the resultant core heating efficiency are low. On the other hands, in the too long scale case ($\gg 1\mu\text{m}$), it takes long time to steepen the density at the LPI region, which means the wide underdense plasma remains in long time. The generated fast electrons energy is hence so high that the confinement effects due to the density gap at the rear surface of cone tip becomes weak. Then the number of relatively low energy fast electrons ($E_{fe} < 2\text{MeV}$), which mainly contributes to the core heating, is decreased, and the core heating efficiency becomes low. It is found that the optimum scale length of pre-plasma is $L_f = 1.5\mu\text{m}$ when the heating pulse intensity is 10^{20}W/cm^2 and the duration is 1ps. In this case, we obtained the energy coupling from heating laser to core of 14.9% and heated core temperature of 0.86keV.

As the results of the radiation–hydro simulations for low intensity LPI, the pre-plasma has a double scale length; a long scale length ($\sim 10\mu\text{m}$) in the underdense region and a short scale length ($\sim 1\mu\text{m}$) in the overdense region. It was found that in the double scale length case, the density steepening is characterized by the scale length of overdense region since the underdense plasma is rapidly swapped out. Thus, the spectrum of fast electrons generated in the double scale length case is almost the same as that in the single short scale length case except for the low energy region ($E_{fe} < 2\text{MeV}$). The number of electrons in the low energy region is slightly large in the double scale case because of the increase in the gap effect. As the results, we found that the core heating efficiencies and the resultant core temperatures become high compared with those in the single scale length case, *e.g.*, the energy coupling from heating laser to core of 16.7% and heated core temperature of 0.94keV are obtained when the scale length of underdense and overdense region are assumed as $5\mu\text{m}$ and $1.5\mu\text{m}$. The obtained ion temperature is almost the same as that measured at the experiment [2].

The above results indicate that the pre-pulse profile (both the spatial and temporal profiles) of the heating laser, which determines the pre-plasma structure, is very important when the heating pulse duration is $\sim 1\text{ps}$. Even in the longer pulse case such as the heating laser at FIREX-I (10ps), the pre-plasma scale length affects the fast electron profiles through the density steepening effect at the LPI region and the density gap effect at the rear surface of cone tip. Thus, for further study, in addition to the multi-dimensional features, the estimation of pre-plasma profiles using realistic pre-pulse profile is required.

We also evaluated the fast ion contribution to the core heating. The fast ions (Au, $Z=50$) are also generated by both static potentials at the laser irradiation surface ($\sim 600\text{MeV}$) and at the rear surface density gap ($\sim 100\text{MeV}$). However, these ions do not contribute to the core heating because of the short range.

ACKNOWLEDGMENTS

This work was supported by MEXT, the Grant-in-Aid for Creative Scientific Research (15GS0214) and partially the Grant-in-Aid for Encouragement of Young Scientists (B) (17760666). We are grateful for the support of the computer room of ILE and the cybermedia center at Osaka University.

REFERENCES

- [1] TABAK, M., *et al.*, “Ignition and High Gain with Ultrapowerful Lasers”, *Phys. Plasmas* **1** (1994) 1626-1634.
- [2] R. KODAMA *et al.*, “Fast Heating Scalable to Laser Fusion Ignition”, *Nature* **418** (2002) 933-934.
- [3] MIMA, K., *et al.*, “”, *Proc. of the IAEA Fusion Energy Conference, Lyon, 2002, (IAEA, Vienna, 2002), Paper No. IAEA-CN-94/IF/03.*
- [4] WILKS, S. C., KRUEER, W. L., TABAK, M., LANGDON, A. B., “Absorption of Ultra-Intense Laser Pulses”, *Phys. Rev. Lett.* **69** (1992) 1383-1386.
- [5] PUKHOV, A., MEYER-TER-VEHN, J., “Laser Hole Boring into Overdense Plasma and Relativistic Electron Currents for Fast Ignition of ICF Targets”, *Phys. Rev. Lett.* **79** (1997) 2686-2689.
- [6] LASINSKI, B. *et al.*, “Particle-in-Cell Simulations of Ultra Intense Laser Pulses Propagating Through Overdense Plasma for Fast-Ignitor and Radiography Applications”, *Phys. Plasmas* **6** (1999) 2041-2047.
- [7] SENTOKU, Y., *et al.*, “Magnetic Instability by the Relativistic Laser Pulses in Overdense Plasmas”, *Phys. Plasmas* **7** (2000) 689-695.
- [8] SENTOKU, Y., MIMA, K., KAW, P., NISHIKAWA, K., “Anomalous Resistivity Resulting from MeV-Electron Transport in Overdense Plasma”, *Phys. Rev. Lett.* **90** (2003) 155001.
- [9] SENTOKU, Y., *et al.*, “Laser Light and Hot Electron Micro Focusing Using a Conical Target”, *Phys. Plasmas* **11** (2004) 3083-3087.
- [10] REN, C. *et al.*, “Global Simulation for Laser-Driven MeV electrons in Fast Ignition”, *Phys. Rev. Lett.* **93** (2004) 185004.
- [11] GREMILLET, L., *et al.*, “Filamented Transport of Laser-Generated Relativistic Electrons Penetrating A Solid Target”, *Phys. Plasmas*, **9** (2002) 941-948.
- [12] CAMPBELL, R. B. *et al.*, “Collimation of Petawatt Laser-Generated Relativistic Electron Beams Propagating Through Solid Matter”, *Phys. Plasmas*, **10** (2003) 4169-4172.
- [13] TAGUCHI, T., ANTONSEN, T. M. JR., MIMA, K., “Study of Hot Electron Beam Transport in High Density Plasma using 3rd hybrid-Darwin Code”, *Comput. Phys. Commun.* **164** (2004) 269-278.
- [14] MATSUMOTO, T., TAGUCHI, T., MIMA, K., “Simulation of the Nonlinear Evolution of Large Scale Relativistic Electron Flow in Dense Plasmas”, *Phys. Plasmas* **13** (2006) 052701.
- [15] CAMPBELL, R. B., *et al.*, “Simulation of Heating-Compressed Fast-Ignition Cores by Petawatt Laser-Generated Electrons”, *Phys. Rev. Lett.* **94** (2005) 055001.
- [16] MASON, R., “Heating Mechanisms in Short-Pulse Laser-Driven Cone Targets”, *Phys. Rev. Lett.* **96**, (2006) 035001.
- [17] JOHZAKI, T., *et al.*, “Analysis of Core Plasma Heating by Relativistic Electrons in Fast Ignition”, *Fusion Sci. Technol.* **43** (2003) 428-436
- [18] YOKOTA, T., NAKAO, Y., JOHZAKI, T., MIMA, K., “Two-Dimensional Relativistic Fokker-Planck Model for Core Plasma Heating in Fast Ignition Targets”, *Phys. Plasmas* **13** (2006) 022702.
- [19] SENTOKU, Y., KEMP, A., COWAN, T., “Full Scale Explicit PIC Simulation of Fast Ignition Experiment”, *J. Phys. IV France* **133** (2006) 425-427.
- [20] SAKAGAMI, H., MIMA, K., “Fast Ignition Simulation with Collective PIC Code”, *Inertial Fusion Sciences and Applications 2001 (Proc. 2nd Int. Conf. on Inertial Fusion Sciences and Applications, Koto, 2001), Elsevier, Paris (2001) 380-383.*
- [21] SAKAGAMI, H., MIMA, K., “Interconnection between Hydro and PIC codes for Fast Ignition Simulations”, *Laser Part. Beams* **22** (2004) 41-44.
- [22] NAGATOMO, H., *et al.*, “Analysis of Hydrodynamic Instabilities in Implosion Using High-Accuracy Integrated Implosion Code”, *Inertial Fusion Sciences and Applications 2001 (Proc. 2nd Int. Conf. on Inertial Fusion Sciences and Applications, Koto, 2001), Elsevier, Paris (2001) 140-142.*
- [23] JOHZAKI, T., *et al.*, “Analysis of Core Plasma Heating by Relativistic Electrons in Fast Ignition”, *Fusion Sci. Technol.* **43** (2003) 428-436.
- [24] SAKAGAMI, H., JOHZAKI, T., NAGATOMO, H., MIMA, K., “Fast Ignition Integrated Interconnecting Code Project for Cone-Guided Targets”, *Laser Part. Beams* **24** (2006) 191-198.
- [25] JOHZAKI, T., *et al.*, “Core Heating Analysis of Fast Ignition Targets by Integrated Simulations”, *J. Phys. IV France* **133** (2006) 385-389.
- [26] SENTOKU, Y., COWAN, T.E., KEMP, A., RUHL, H., “High Energy Proton Acceleration in Interaction of Short Laser Pulse with Dense Plasma Target”, *Phys. Plasmas* **10** (2003) 2009-2015.